



**HAL**  
open science

# Mn(III) Chain Coordination Polymers Assembled by Salicylidene-2-ethanolamine Schiff Base Ligands: Synthesis, Crystal Structures, and HFEPR Study

Oleh Stetsiuk, Nataliya Plyuta, Narcis Avarvari, Evgeny Goreshnik, Vladimir Kokozay, Svitlana Petrusenko, Andrew Ozarowski

► **To cite this version:**

Oleh Stetsiuk, Nataliya Plyuta, Narcis Avarvari, Evgeny Goreshnik, Vladimir Kokozay, et al.. Mn(III) Chain Coordination Polymers Assembled by Salicylidene-2-ethanolamine Schiff Base Ligands: Synthesis, Crystal Structures, and HFEPR Study. *Crystal Growth & Design*, 2020, 20 (3), pp.1491-1502. 10.1021/acs.cgd.9b01150 . hal-02913398

**HAL Id: hal-02913398**

**<https://univ-angers.hal.science/hal-02913398v1>**

Submitted on 30 Nov 2020

**HAL** is a multi-disciplinary open access archive for the deposit and dissemination of scientific research documents, whether they are published or not. The documents may come from teaching and research institutions in France or abroad, or from public or private research centers.

L'archive ouverte pluridisciplinaire **HAL**, est destinée au dépôt et à la diffusion de documents scientifiques de niveau recherche, publiés ou non, émanant des établissements d'enseignement et de recherche français ou étrangers, des laboratoires publics ou privés.

This document is confidential and is proprietary to the American Chemical Society and its authors. Do not copy or disclose without written permission. If you have received this item in error, notify the sender and delete all copies.

**Mn(III) Chain Coordination Polymers assembled by Salicylidene-2-ethanolamine Schiff Base Ligands: Synthesis, Crystal Structures and HFEPR Study**

Journal:	<i>Crystal Growth &amp; Design</i>
Manuscript ID	cg-2019-01150x.R2
Manuscript Type:	Article
Date Submitted by the Author:	16-Jan-2020
Complete List of Authors:	Stetsiuk, Oleh ; University of Angers Plyuta, Nataliya; University of Angers; Taras Shevchenko National University of Kyiv Avarvari, Narcis; Universite d'Angers, Chemistry Goreshnik, Evgeny; Institut Jozef Stefan, Inorganic Chemistry and Technology Kokozay, Vladimir; Kyyivs'kij nacional'nij universytet imeni Tarasa Shevchenka, Department of Chemistry Petrusenko, Svitlana; Taras Shevchenko National University of Kyiv, Chemistry Ozarowski, Andrew; Florida State University, Natl High Magnet Field Lab

SCHOLARONE™  
Manuscripts

1  
2  
3  
4  
5  
6  
7  
8  
9  
10  
11  
12  
13  
14  
15  
16  
17  
18  
19  
20  
21  
22  
23  
24  
25  
26  
27  
28  
29  
30  
31  
32  
33  
34  
35  
36  
37  
38  
39  
40  
41  
42  
43  
44  
45  
46  
47  
48  
49  
50  
51  
52  
53  
54  
55  
56  
57  
58  
59  
60

# **Mn(III) Chain Coordination Polymers assembled by Salicylidene–2– ethanolamine Schiff Base Ligands: Synthesis, Crystal Structures and HFEPR Study**

Oleh Stetsiuk<sup>a</sup>, Nataliya Plyuta<sup>a,c</sup>, Narcis Avarvari<sup>a</sup>, Evgeny Goreshnik<sup>b</sup>, Vladimir Kokozay<sup>c</sup>,  
Svitlana Petrusenko<sup>\*c</sup>, and Andrew Ozarowski<sup>\*d</sup>

<sup>a</sup>*MOLTECH–Anjou, UMR 6200, CNRS, UNIV Angers, 2 bd Lavoisier, 49045 ANGERS Cedex,  
France*

<sup>b</sup>*Department of Inorganic Chemistry and Technology, Jožef Stefan Institute, Jamova 39, 1000  
Ljubljana, Slovenia*

<sup>c</sup>*Department of Inorganic Chemistry, Taras Shevchenko National University of Kyiv,  
Volodymyrska str. 64/13, Kyiv 01601, Ukraine. E–mail: spetrusenko@yahoo.com*

<sup>d</sup>*National High Magnetic Field Laboratory, Florida State University, 1800 E. Paul Dirac Drive,  
Tallahassee, Florida 32310, USA. E–mail: ozarowsk@magnet.fsu.edu; Fax: +1 850–644–1366*

## Abstract

A family of eight polymeric manganese (III) complexes with the general formula  $\text{Mn}(\text{HL}^{1,2})_2\text{X}$ , ( $\text{H}_2\text{L}^1 = 2[(2\text{-hydroxyethyl})\text{iminomethyl}]\text{phenol}$ ,  $\text{H}_2\text{L}^2 = 2[(2\text{-hydroxyethyl})\text{iminomethyl}]\text{-6-methoxy-phenol}$ ) while  $\text{X} = \text{Cl}$  (**1**, **5**),  $\text{Br}$  (**2**, **6**),  $\text{I}$  (**3**, **7**),  $\text{NCS}$  (**4**, **8**) for  $\text{H}_2\text{L}^1$  and  $\text{H}_2\text{L}^2$ , respectively were obtained using “the direct synthesis” approach, i.e., the oxidative dissolution of the manganese powder in the presence of a Schiff base (SB), an ammonium salt and oxygen of the air. Single crystal X-ray diffraction studies for the new complexes **2**, **3**, **4** and **8** were compared with the previously reported crystallographic data for **1** and **7**, showing that all complexes possess 1D polymeric structure. The main structural units in **1–7** are cationic chains  $[\text{Mn}(\text{HL}^{1,2})_2]_n^{n+}$  and anions  $\text{X}^-$  linked together *via* electrostatic interactions and hydrogen bonds, while the complex **8** consists of polymeric chains of neutral  $[\text{Mn}(\text{HL}^2)_2(\text{NCS})]_n$  units. The SB ligands are mono-deprotonated as  $\text{HL}^-$ , and coordinated by the metal atoms in a tridentate chelate-bridging fashion generating chains with Mn centers connected by double or single  $\{-\text{N}-\text{C}-\text{C}-\text{O}-\}$  bridges for **1–7** and **8**, respectively. In **8** bridging and pure chelate modes of  $\text{HL}^{2-}$  occur. The intra-chain  $\text{Mn}^{\text{III}}\cdots\text{Mn}^{\text{III}}$  distances vary from 5.700(2) Å for **1** to 6.6950(4) Å for **8**. The High-Field EPR study reveals narrow ranges of the zero-field splitting parameters of the spin Hamiltonian,  $D$  and  $E$  ( $-3.22\text{ cm}^{-1}$  to  $-3.44\text{ cm}^{-1}$  and  $-0.16\text{ cm}^{-1}$  to  $-0.21\text{ cm}^{-1}$ , respectively) and demonstrates a clear correlation between the degree of the structural distortion and the  $E$  parameter. The *ab-initio* CASSCF method was employed to calculate the zero-field splitting parameters. “Broken symmetry” DFT calculations were performed to estimate the magnitude of the Mn–Mn exchange interactions.

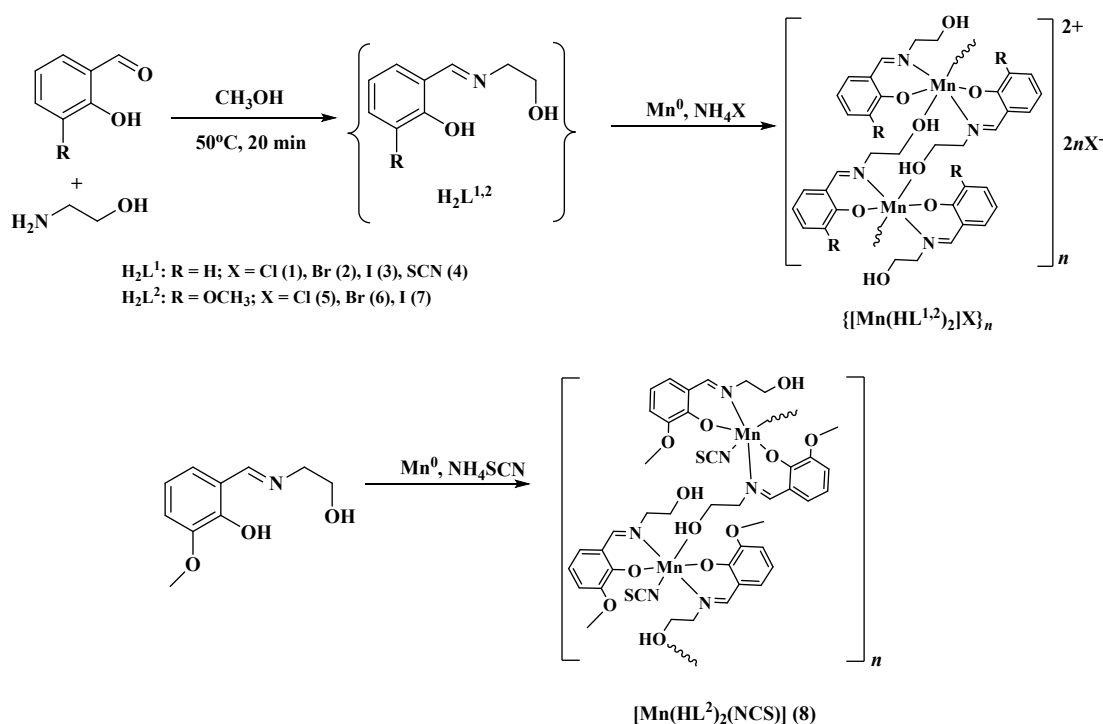
## Introduction

The coordination chemistry of manganese (III) attracts persistent attention mainly for its principal role in the important catalytic cycles in Nature.<sup>1-3</sup> In addition, a special interest in this subject has been caused by the discovery of SMM (single-molecule magnet) behavior in the mixed (III, IV) valence complex  $[\text{Mn}_{12}\text{O}_{12}(\text{O}_2\text{CCH}_3)_{16}(\text{H}_2\text{O})_4]$ .<sup>4</sup> The electronic configuration of Mn(III) centers with  $S=2$  ground spin state  $t_{2g}^3e_g^1$  and a strong axial magnetic anisotropy resulting from the Jahn-Teller effect, make them potentially good candidates for demonstration of SMM (single molecule magnet),<sup>5</sup> SIM (single ion magnet)<sup>6-9</sup> and SCM (single chain magnets)<sup>10-13</sup> properties and, thus, for the creation of the high information density storage materials. At the same time, the development of the Mn(III) chemistry has not been satisfactory because of the synthetic problems associated with Mn(III) disproportionation processes and the formation of insoluble and very stable  $\text{MnO}_2$ .<sup>14</sup> Herein, we report a simple and effective synthetic route to a series of the cationic and molecular polymeric Mn(III) chain complexes  $\{[\text{Mn}(\text{HL}^{1,2})_2]\text{X}\}_n$  (**1-7**) and  $[\text{Mn}(\text{HL}^2)_2(\text{NCS})]_n$  (**8**), ( $\text{H}_2\text{L}^1 = 2[(2\text{-hydroxyethyl)iminomethyl]phenol}$ ,  $\text{H}_2\text{L}^2 = 2[(2\text{-hydroxyethyl)iminomethyl]-6\text{-methoxyphenol}$ ;  $\text{X} = \text{Cl}, \text{Br}, \text{I}, \text{NCS}$ ) as well as a detailed investigation of the complexes by X-ray crystallography, FTIR and HF EPR methods, combined with density functional theory (DFT) calculations.

## Results and discussion

### Synthesis, spectroscopic analysis and crystal structures of manganese complexes

The general synthetic route is depicted in Scheme 1. The Schiff base ligands  $H_2L^1$  and  $H_2L^2$  were prepared *in situ* by condensation of 2-aminoethanol with salicylaldehyde or *o*-vanillin, respectively. Manganese complexes **1–8** were obtained *via* the “direct synthesis” (DS) approach, which is based on using regular metal powders instead of their salts as a source of metal. This method has been widely investigated by our group<sup>15,16</sup> and it has been shown that in some cases there are advantages in exploiting DS conditions as compared to the traditional “wet” chemistry. For example, a better morphology of the crystal products and absence of contaminating anions were noticed. At the same time, there is a possibility to obtain complexes with the metals whose salts are very expensive or commercially unavailable as starting materials.<sup>17,18</sup> It should be noted that a synthesis of complex **1** by using metal salt as a precursor was previously reported.<sup>19</sup> All DS reactions were performed by heating and magnetic stirring in open air. Total dissolution of the metal powders indicated the reaction end. Crystals suitable for X-ray analysis were formed within few days when the resulting brown solutions were allowed to stand at room temperature. For the complexes  $[Mn(HL^2)_2]Cl$  (**5**) and  $[Mn(HL^2)_2]Br$  (**6**) the single crystals have not been obtained and their composition was confirmed by elemental analysis, FTIR and HF EPR methods. It is noteworthy that in the systems with an ammonium thiocyanate, two different complexes with the same composition  $Mn(HL^{1,2})_2(NCS)$  but different crystal structure were obtained (Scheme 1).



### Scheme 1. Synthesis of manganese complexes 1–8.

The IR spectra of compounds **1–8** show similar absorption bands and confirm the presence of the Schiff base ligands. Very strong bands in the region 1599–1649  $\text{cm}^{-1}$  were assigned to the double imino (C=N) bonds vibrations. The broad bands in the region 3400–3100  $\text{cm}^{-1}$  indicate the presence of hydroxo groups, which are partially deprotonated in all complexes. Non-coordinated and coordinated thiocyanate anion in **4** and **8** are confirmed by the presence of the intense peaks (C=N) at 2055 and 2071  $\text{cm}^{-1}$  and weak (C–S) vibrations at 760 and 784  $\text{cm}^{-1}$ , in **4** and **8**, respectively.

X-ray crystal structures were determined for the compounds **2–4** and **8** (Table 6), and those for **1** and **7** have been reported earlier.<sup>19,20</sup> All complexes are 1D polymers based on Mn(III) centers. The crystal lattices of the halogenide complexes are similar and consist of the cationic chains  $[\text{Mn}(\text{HL}^{1,2})_2]^+$  (Figure 1) and counter ions  $\text{X}^-$  (Cl, Br, I), while the thiocyanate complexes possess both cationic (**4**) and neutral chain (**8**) structures depending on the ligand used (Figure 2–3). In the case of compound **4** packing of above-mentioned chains containing inversion centers and acentric  $\text{SCN}^-$  anions results in the chiral  $P2_12_12_1$  space group.

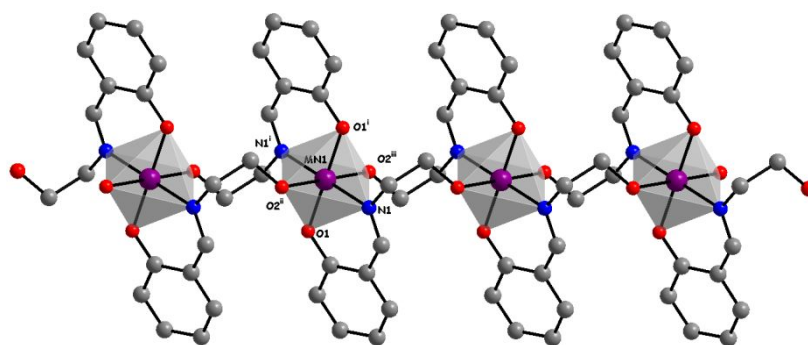


**Figure 1.** Crystal structure of the polymeric cation  $[\text{Mn}(\text{HL}^{1,2})_2]^{n+}$  in **1–4** and **7**. Hydrogen atoms and methoxy groups are omitted. Symmetry operations: (i)  $-x, -y, -z$ ; (ii)  $x, 1+y, z$ ; (iii)  $-x, -1-y, -z$ .

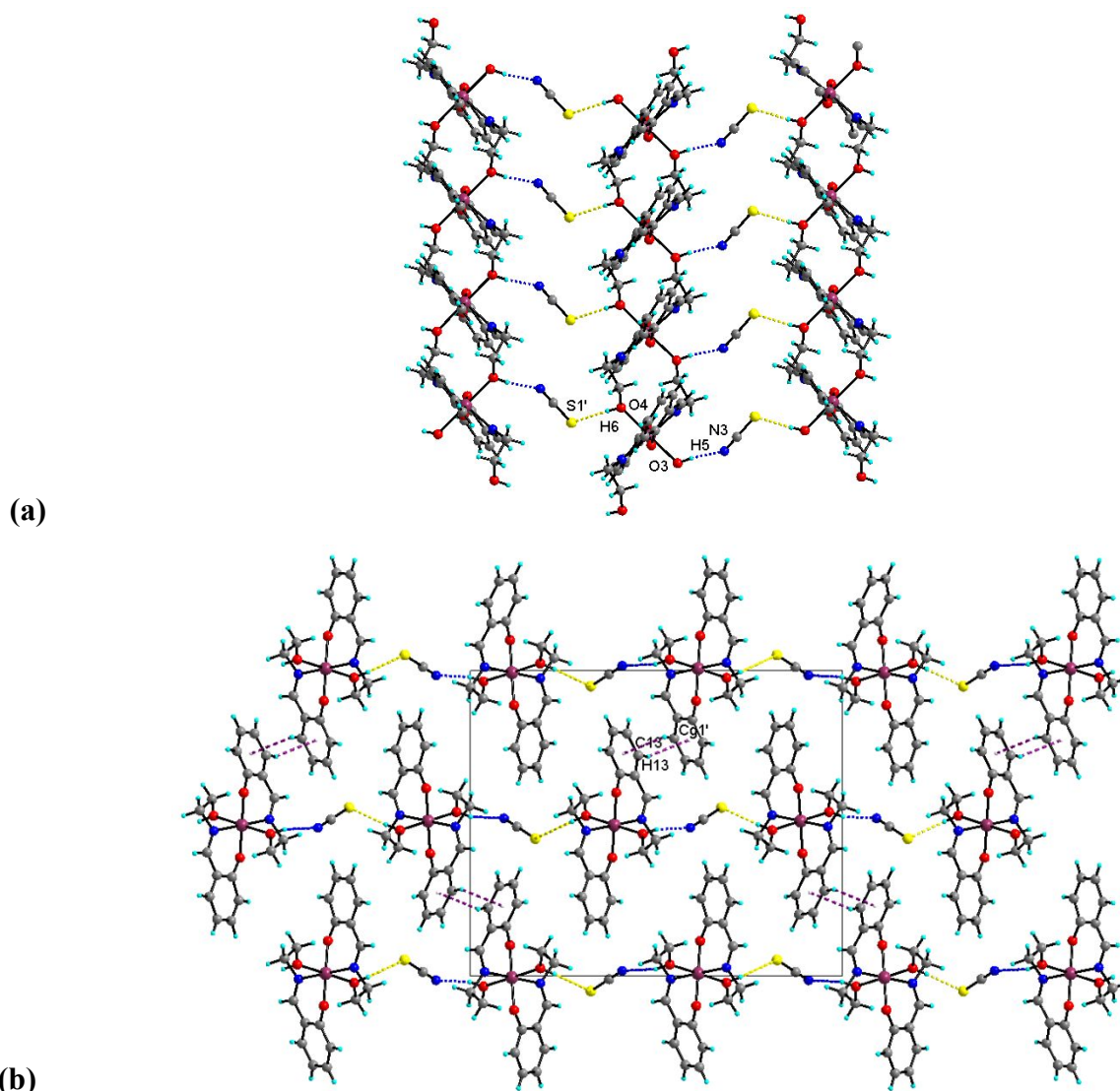
The metal atoms are hexacoordinated with  $[\text{N}_2\text{O}_4]$  or  $[\text{N}_3\text{O}_3]$  environments typical for Mn(III) pseudo-octahedral (4+2) geometry. The deviation from ideal  $O_h$  symmetry relates mainly to linear parameters of the metal coordination polyhedra (the differences in the bond lengths being of more than 0.4 Å) and is negligible for angular parameters with maximal values observed for **8** (Table 1). The +3 manganese oxidation state is readily seen in the EPR spectra (see below), as signals of an  $S = 2$  spin state are detected. This was also confirmed by comparison of coordination bond distances, existence of Jahn–Teller elongation, and bond valence sum calculation (Table 1).

**Table 1. Comparison of geometrical parameters of the Mn coordination polyhedra in 1–4 and 8.**

	$H_2L^1$				$H_2L^2$	
	<b>1*</b>	<b>2</b>	<b>3</b>	<b>4</b>	<b>7*</b>	<b>8</b>
Mn—O (short), Å	1.866(2)	1.873(1)	1.871(1)	1.861(3) 1.876(3)	1.829(8) 1.849(8)	1.844(2) 1.864(2)
Mn—O (long), Å	2.287(2)	2.287(2)	2.288(1)	2.242(3) 2.282(3)	2.247(8) 2.315(8)	2.340(2)
Mn—N, Å	2.023(2)	2.029(2)	2.026(2)	2.037(4) 2.049(4)	2.040(1) 2.061(9)	2.031(2) 2.053(2) 2.231(2)
$\Delta_{max}^{**}$ , Å	0.421(2)	0.414(2)	0.417(2)	0.421(4)	0.418(9)	0.496(2)
BVS <sup>***</sup>	3.05	3.00	3.02	3.01	3.08	3.13
<i>trans</i> -angles, °	180	180	180	177.9(2) 178.9(1) 179.1(2)	179.0(4) 179.2(5) 179.5(5)	178.43(7) 173.02(7) 178.39(7)
$\Delta_{max}$ , °	0	0	0	2.1(2)	1.0(5)	5.41(7)
<i>cis</i> -angles, °	87.29(7)– 92.71(7)	86.97(6)– 93.03(6)	87.33(5)– 92.67(5)	87.5(1)– 93.6(1)	86.8(3)– 92.5(4)	84.78(6)– 93.89(7)
$\Delta_{max}$ , °	5.42(7)	6.06(6)	5.34(5)	6.1(1)	5.7(4)	9.11(7)
*The crystallographic data for 1 and 7 were previously reported in 19 and 20, respectively.						
** $\Delta_{max}$ – the difference between a maximal and a minimal bond length or angle.						
***BVS – bond valence sum for Mn atoms. <sup>21,22</sup>						

The one-dimensional polymeric structure is achieved due to chelate-bridging function of the ligands,  $[2.01_11_11_2]$  by Harris notation.<sup>23</sup> The cationic chains along with bridging  $X^-$  anions located on inversion centers form H-bond based layers parallel to *ab* plane which are further interconnected by C–H... $\pi$  bonds between  $HL^-$  rings to yield a 3D supramolecular architecture (Figure 4; Table 2, 3).





39 **Figure 2.** Crystal structure of **4**: (a) H-bonded layers; and (b) projection of crystal packing viewing along the [100]  
40 direction. Symmetry operations: (a) (i)  $1.5-x, 1-y, 0.5+z$ ; (b)  $Cg1'$  is a centroid of C9...C14 benzene ring (i)  $1-x,$   
41  $0.5+y, 0.5-z$ .

42  
43 The maximum similarity of the crystal structure is observed for the halide complexes with  
44  $H_2L^1$  (**1–3**), nevertheless they are not isostructural. There is a direct correlation between the size  
45 of the halogen atom and the intra-chain  $Mn \cdots Mn$  distance as increasing the radius of the ion  
46 halide in the sequence  $Cl^- (1.81 \text{ \AA}) < Br^- (1.97 \text{ \AA}) < I^- (2.23 \text{ \AA})$ <sup>24</sup> leads to the interatomic distance  
47 increase by approximately  $0.02 \text{ \AA}$  (Table 3). But for the complex **4** with  $NCS^-$ , which is the  
48 largest anion in the sequence, the  $Mn \cdots Mn$  distance is somewhat smaller than expected which  
49 can be explained by a different way of crystal packing with  $C-H \cdots \pi$  interactions between the  
50 aromatic rings of  $H_2L^1$  (Figure 2, Table 3).  
51  
52  
53  
54  
55  
56  
57  
58  
59  
60

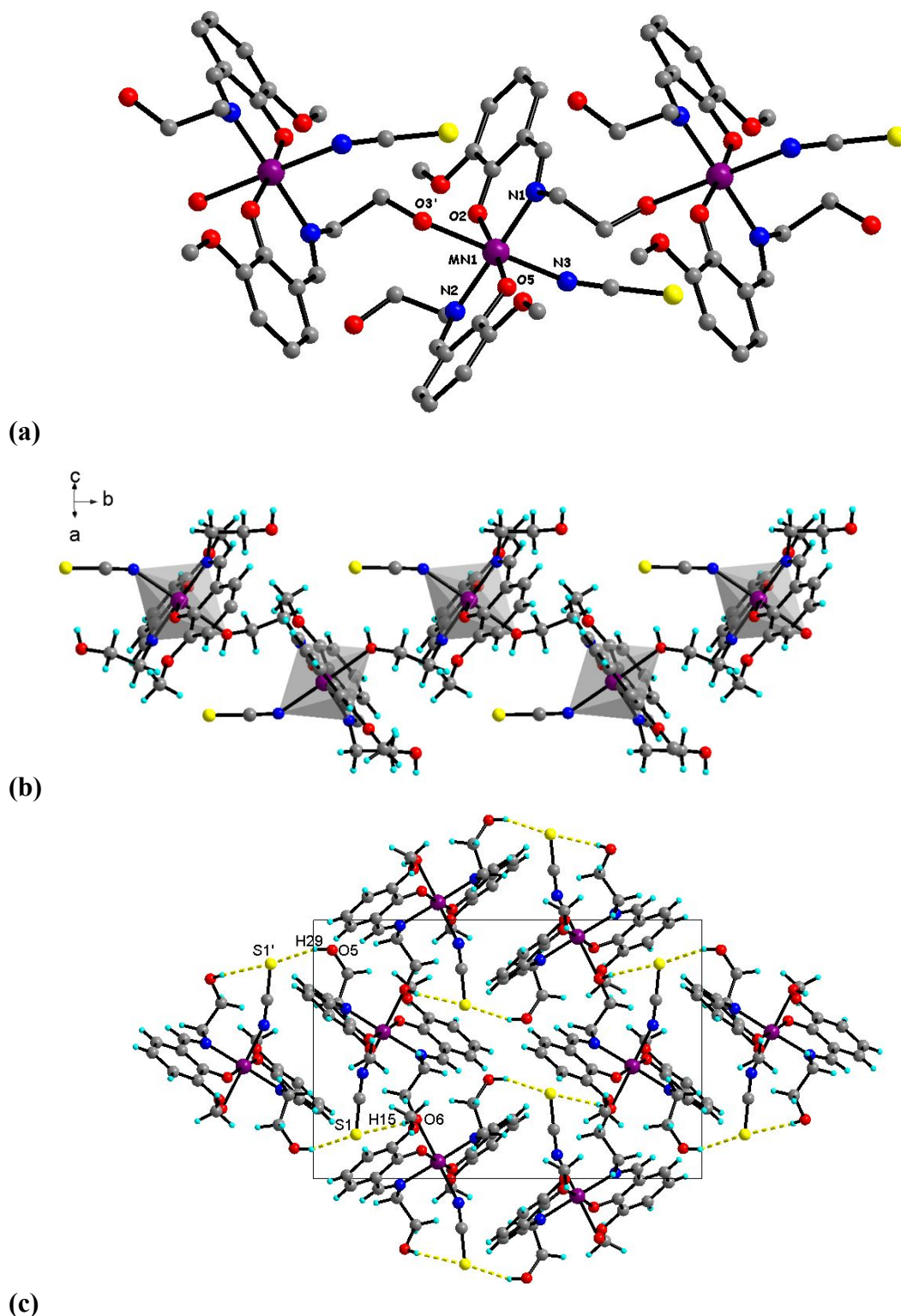


**Figure 3.** Crystal structure of **8**: (a) molecular structure with labeling scheme; (b) fragment of polymeric chain  $[\text{Mn}(\text{HL}^2)_2(\text{NCS})]_n$  and (c) projection of crystal packing viewing along  $[010]$  direction. Symmetry operations: (a) (i)  $1.5-x, -0.5+y, 1.5-z$ ; (c) (i)  $1-x, 1-y, 2-z$ .

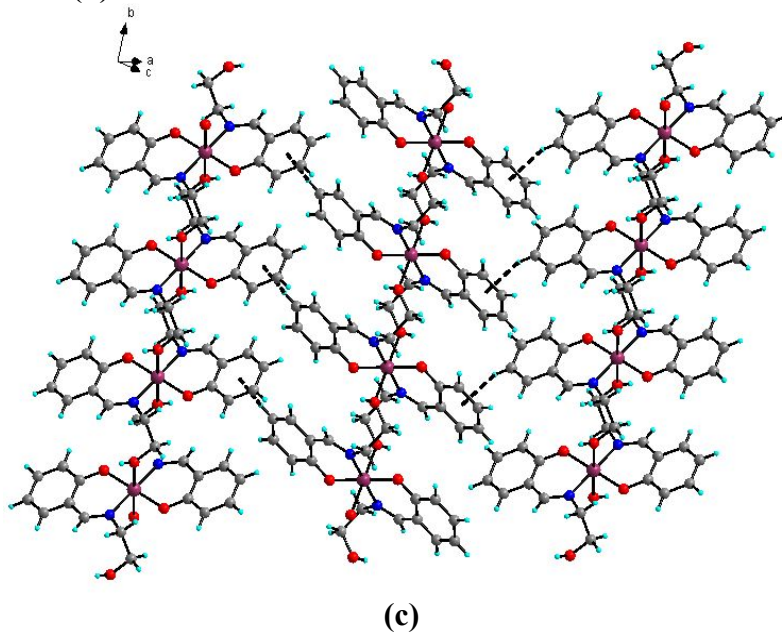
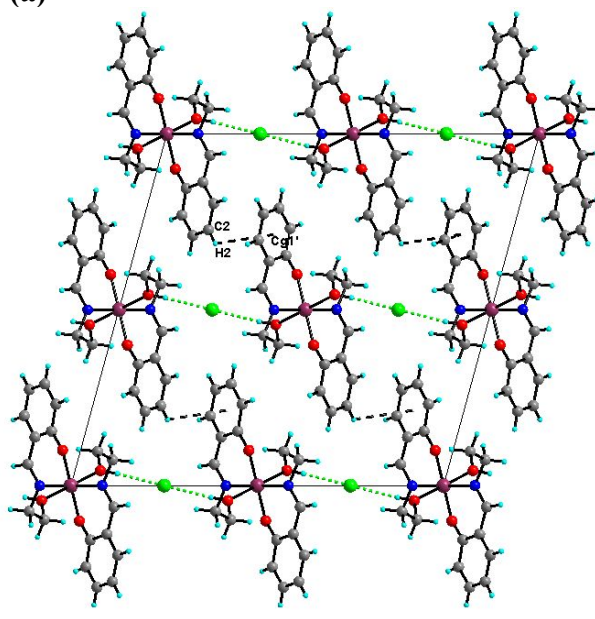
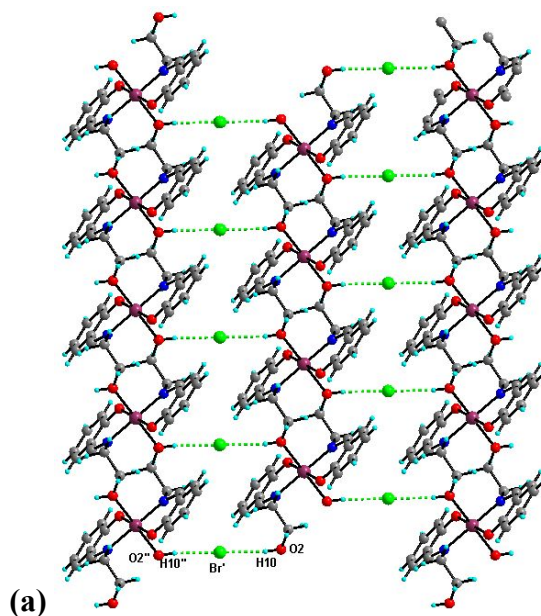


**Figure 4.** Crystal structure of **2**: (a) H-bonded layers; (b) projection of crystal packing viewing along [010] direction; (c) layers based on C–H... $\pi$  bonds. Symmetry operations: (a) (i)  $-x, -1+y, 0.5-z$ ; (ii)  $-0.5-x, -1.5-y, -z$ ; (b) Cg1' is a centroid of C1...C6 benzene ring (i)  $x, 1-y, -0.5+z$ .

The presence of a bulky methoxy group in the benzene ring of  $H_2L^2$  has a noticeable effect on the packing of the iodide complex **7**, where the polymeric cations and iodide anions form H-bonded chain supramolecular frame unlike the layer found in the halide complexes with  $H_2L^1$  (Figure 5).

The most drastic differences are observed when replacing the SB ligand in the thiocyanate complex: instead of the cationic complex  $[Mn(HL^1)_2]NCS$  **4**, a neutral complex of the analogous composition  $[Mn(HL^2)_2(NCS)]$  **8** was obtained (Figure 3). In **8** the  $\{MnN_3O_3\}$  chromophore is formed by two monodeprotonated SB ligand molecules with different coordination modes (*N,O*-chelated and *O,N,O'*-bridging-chelate) and *N*-coordinated thiocyanate group. The metal atom shifted from the equatorial plane by *ca* 0.07 Å towards  $N_{NCS}$ . The manganese atoms in  $\{Mn\}_n$  chains are arranged in a zigzag fashion with  $Mn \cdots Mn$  distance of 6.7 Å and the Mn–Mn–Mn angles of 121.3°.

Each non-coordinated S-donor atom from the NCS group forms two H-bonds with OH groups from aminoalcohol arms of the bridging SB ligand (intra-HB) and the chelate ligand (inter-HB) (Figure 3, Table 2).

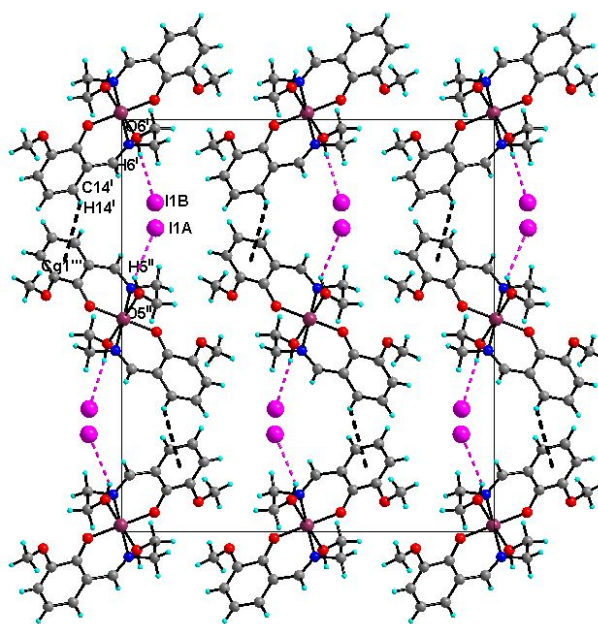


**Figure 5.** Projection of crystal packing of **7** viewing along the [010] direction. Symmetry operations: (i)  $x, 1+y, z$ ; (ii)  $-x, 1-y, 0.5+z$ ; Cg1' is a centroid of C1...C6 benzene ring (iii)  $0.5-x, -2+y, -0.5+z$ .

**Table 2.** Hydrogen bonds parameters in **1–4, 7, 8**.

1			
D—H...A	H...A	D...A	D—H...A
O2—H10...Cl	2.299(1)	3.057(2)	164(2)
2			

O2—H10…Br1'	2.42(1)	3.265(2)	173(3)
<b>3</b>			
O2—H5…I1'	2.66(1)	3.508(1)	172(3)
<b>4</b>			
O3—H5…N3	1.88(4)	2.706(5)	162(8)
O4'—H6'…S1	2.31(6)	3.154(3)	175(9)
<b>7</b>			
O5''—H5''…I1A	2.863(1)	3.488(8)	131(6)
O6'—H6'…I1B	2.620(4)	3.477(9)	173(6)
<b>8</b>			
O5—H29…S1'	2.66(3)	3.426(2)	155(3)
O6'—H15'…S1'	2.60(3)	3.347(2)	167(3)
Symmetry transformations used to generate equivalent atoms: <b>(2)</b> (i) $-x, -1+y, 0.5-z$ ; <b>(3)</b> (i) $-0.5+x, -0.5+y, z$ <b>(4)</b> (i) $1.5-x, 1-y, 0.5+z$ <b>(7)</b> (i) $x, 1+y, z$ , (ii) $-x, 1-y, 0.5+z$ ; <b>(8)</b> (i) $1-x, 1-y, 2-z$ .			

**Table 3. Selected C–H… $\pi$  interactions and Mn…Mn distances in 1–4 and 7, 8.**

	$H_2L^1$				$H_2L^2$	
	<b>1(Cl)</b>	<b>2 (Br)</b>	<b>3 (I)</b>	<b>4 (NCS)</b>	<b>7(I)</b>	<b>8(NCS)</b>
C–H… $\pi$ , Å	2.806(1)	3.2020(2)	3.3206(1)	2.5930(1)	3.4252(3)	–
Mn…Mn, Å	5.700(2)	5.7196(3)	5.7552(2)	5.7247(9)	5.898(4)	6.6950(4)

### High-Field EPR Spectra

The ground state of the Mn(III) ion is the even-spin  $S=2$  state and complexes containing Mn(III) exhibit typically large zero-field splitting with the  $D$  parameter of the spin Hamiltonian (1) of a few  $\text{cm}^{-1}$ , making them very difficult to investigate by standard EPR, as the small microwave quantum energy cannot cause transitions between the  $M_S$  levels

$$\hat{H} = \mu_B \mathbf{B}\{\mathbf{g}\}\hat{\mathbf{S}} + D \left\{ \hat{S}_z^2 - \frac{1}{3}S(S+1) \right\} + E(\hat{S}_x^2 - \hat{S}_y^2) + B_4^0 O_4^0 + B_4^4 O_4^4 \quad (1)$$

Interestingly, there is one exception to this: the  $M_S=2$  and  $M_S=-2$  levels of the  $S=2$  state are split very little in the absence of the magnetic field (approximately  $3E^2/D$ ) and a nominally “forbidden”  $\Delta M_S=4$  transition sometimes appears in X-Band EPR at an effective  $g$  value of  $\sim 8$ .<sup>2,25–29</sup> The transition under question is however only weakly sensitive to the  $D$  parameter. High-field and high-frequency EPR (HF-EPR) offers an effective remedy to these problems.<sup>30–33</sup> The microwave quantum energies available to us are up to  $\sim 20 \text{ cm}^{-1}$  ( $\sim 600 \text{ GHz}$ ) and allow observation of all possible transitions in Mn(III) systems. Complexes of Mn(III) tend to produce HF-EPR spectra of good quality. Out of the eight complexes studied in this work, **1**, **2**, **4**, **5** and **6** behaved very well, while the two iodide-containing species **3** and **7** as well as complex **8**, containing thiocyanate coordinated to Mn, posed problems (see below). Figure 6 shows spectra of **5** recorded at 15 K with various microwave frequencies.

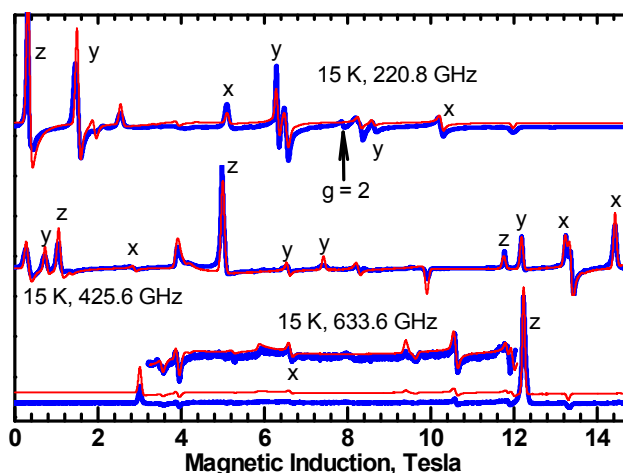


**Figure 6.** EPR spectra of **5** recorded at conditions indicated. Blue: experimental; red: simulated using parameters from Table 5. Labels x, y and z indicate the molecular orientation at which a transition occurs. The unlabeled features correspond to the off-axis turning points.

To determine the spin Hamiltonian parameters accurately, a large number of spectra were recorded and the resonance fields were plotted versus the microwave frequency (Fig. 7 for complex **5**). The dependencies so obtained were fitted, resulting in the spin Hamiltonian parameters in Table 4. Taking into account the quartic parameters of spin Hamiltonian (1),  $B_0^4$  and  $B_4^4$  had a very small effect on the fit quality and on other parameters.

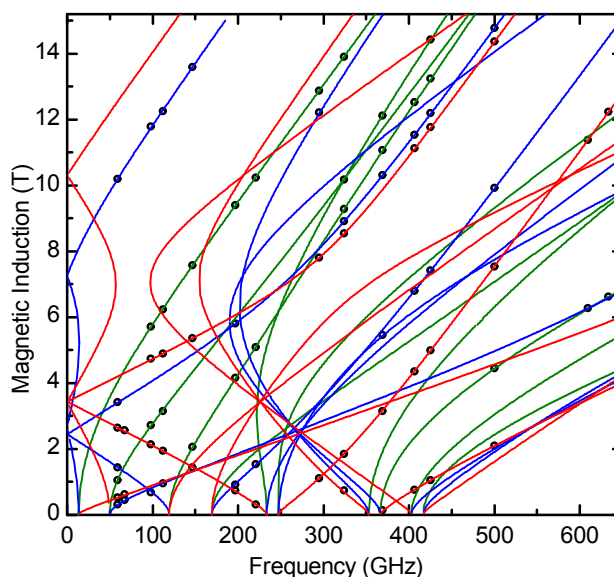


**Figure 7.** Frequency dependencies of the resonance fields corresponding to the canonical transitions in **5**. Circles: experimental resonance positions; green, blue and red lines: calculated X, Y and Z resonances, respectively. The lines with the highest slope represent the “allowed”  $\Delta M_S=1$  transitions. The plots of the “forbidden” transitions ( $\Delta M_S>1$ ) have lower slopes.

An additional advantage of HF-EPR is the easy  $D$  sign determination. The positions of the EPR transitions do not depend on the sign of  $D$  or  $E$  in eq. 1, but spectra taken at low temperatures exhibit an intensity pattern depending on the sign, resulting in complete freezing out of certain transitions, as shown in Fig. 8. This effect depends on the magnitude of the Zeeman energy rather than on the  $D$  magnitude and the sign of a small  $D$  can also be determined.<sup>34–36</sup>

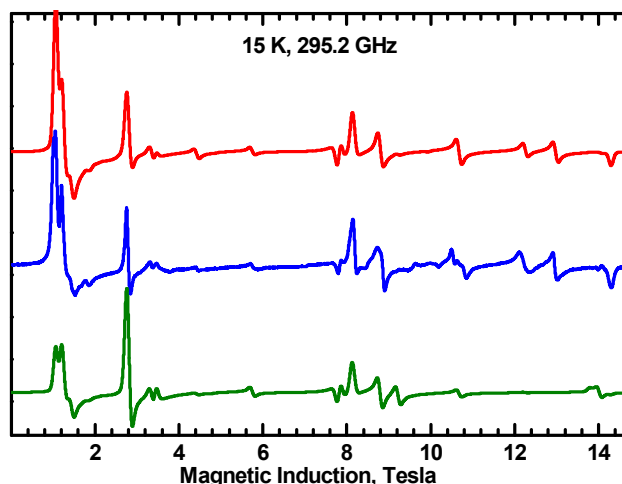


**Figure 8.** HF-EPR spectrum of **4**. Blue: experimental; red: simulated using parameters from Table 4; green: simulated with the signs of  $D$  and  $E$  inverted.

**Table 4. Experimental spin Hamiltonian parameters<sup>1</sup>**

Complex	$g_x$	$g_y$	$g_z$	$D$ (cm <sup>-1</sup> )	$E$ (cm <sup>-1</sup> )	$B_4^0$ (cm <sup>-1</sup> )	$B_4^4$ (cm <sup>-1</sup> )
<b>1</b> <sup>2</sup> (H <sub>2</sub> L <sup>1</sup> )	1.982(4)	1.985(4)	1.998(2)	-3.231(2)	-0.578(2)	0	-0.002(1)
<b>2</b> (H <sub>2</sub> L <sup>1</sup> )	1.980(2)	1.974(2)	1.988(3)	-3.223(3)	-0.548(2)	-0.0006(1)	0.003(1)
<b>3</b> (H <sub>2</sub> L <sup>1</sup> )	1.984(4)	1.963(3)	1.998(5)	-3.197(3)	-0.525(3)		0
<b>4</b> (H <sub>2</sub> L <sup>1</sup> )	1.998(1)	1.986(1)	1.992(2)	-3.296(3)	-0.662(2)	-0.0003(1)	-0.0019(1)
<b>5</b> (H <sub>2</sub> L <sup>2</sup> )	2.001(2)	1.997(1)	1.998(2)	-3.271(2)	-0.663(1)	-0.0001(1)	-0.0034(5)
<b>6</b> (H <sub>2</sub> L <sup>2</sup> )	1.999(1)	1.997(1)	2.000(1)	-3.290(2)	-0.699(2)	-0.0003(1)	-0.0006(3)
<b>7</b> (H <sub>2</sub> L <sup>2</sup> )	1.999(9)	1.961(4)	1.990(6)	-3.34(1)	-0.76(1)	0	0
<b>8</b> (H <sub>2</sub> L <sup>2</sup> )	2.00(1)	1.97(1)	1.96(1)	-3.44(1)	-0.77(1)	0	0

<sup>1</sup> Zero values of  $B_4^0$  and  $B_4^4$  indicate that they have not been fitted. <sup>2</sup>A 1-year old sample of **1** exhibited slightly altered spin Hamiltonian parameters (see Fig. S1).

Complex **8** differs from other ones by having an SCN<sup>-</sup> anion coordinated to Mn, it is thus interesting to compare its spin Hamiltonian parameters to those of the remaining compounds in which the anions are non-coordinated. Unlikely most other systems (except for **7**), difficulties were encountered in recording the EPR spectra of **8**. The compressed powder samples exhibited too many features, which could not be explained within the monomeric Mn<sup>3+</sup> model (Fig. S4).

1  
2 These features were also present when using eicosane pellets with dispersed powder of **8**, thus  
3 eliminating the possibility that they were due to magnetic torquing. A subset of resonances could  
4 be found whose frequency dependencies allowed to determine the parameters of **8** in Table 4.  
5 Other spectral features may be due to weak interactions between the Mn(III) ions. The  $D$  value in  
6 **8** was the largest in the series, but the differences along the series were not dramatic. The  $D$   
7 parameter ranges from  $-3.197$  to  $-3.44$   $\text{cm}^{-1}$  (Table 4), which is just a 7% change. The  $E$   
8 parameter shows a larger relative variation, from  $-0.525$  in **3** to  $-0.77$   $\text{cm}^{-1}$  in **8**. The  $E$  parameter  
9 tends to be larger in the  $\text{H}_2\text{L}^2$  ligand complexes, in agreement with the generally more distorted  
10 structures compared to those of  $\text{H}_2\text{L}^1$  ligand.  
11  
12  
13  
14  
15  
16  
17  
18

### 19 **Calculations of the Zero-Field Splitting**

20  
21 The zero-field splitting (zfs) is a result of spin-orbit coupling and ligand field splitting of energy  
22 levels of a paramagnetic atom possessing spin larger than  $\frac{1}{2}$ . Dependencies between the zfs  
23 parameters and the ligand-field energies for various electronic configurations are well known.<sup>37–</sup>  
24  
25  
26  
27  
28  
29  
30  
31  
32  
33  
34  
35  
36  
37  
38  
39  
40  
41  
42  
43  
44  
45  
46  
47  
48  
49  
50  
51  
52  
53  
54  
55  
56  
57  
58  
59  
60  
The  $^5\text{D}$  term of the Mn(III) ion in an elongated tetragonal bipyramid gives rise to a  $^5\text{B}_{1g}$   
ground state and the  $D$  parameter is usually negative, with rare exceptions.<sup>40,41</sup> The excited states  
contributing to the zero-field splitting via the spin-orbit coupling are  $^5\text{E}_g$  and  $^5\text{B}_{1g}$  states, derived  
from  $^5\text{D}$  free-ion term, and the  $^3\text{E}_g$  state derived from the  $^3\text{H}$  term. The ligand-field splittings  
which are needed to relate the spin Hamiltonian parameters to the electronic spectra, are  
typically difficult to obtain due to the presence of intense  $\pi$ - $\pi^*$  and charge transfer bands. In  
more recent years, Density Functional Theory (DFT) and *ab initio* methods have been applied to  
get insight into the nature of the zero-field splitting.<sup>41–43</sup> It is now believed that the contribution  
of the spin-spin interactions to the zero-field splitting is not necessarily negligible compared to  
the spin-orbit coupling contribution. We have attempted to calculate the spin-orbit coupling  
contribution to  $D$  and  $E$  in our complexes using the state-averaged complete active space self-  
consistent field (CASSCF)<sup>41–43</sup> approach, with four electrons in 5 orbitals. 5 quintet and lowest  
35 triplet states were taken into account, like in refs 41–43. Functional B3LYP was employed  
with TZVPP functions for Mn and all coordinated atoms and SVP functions for all remaining  
atoms.<sup>44–46</sup> Calculations were performed using the ORCA software package.<sup>47</sup> The spin-spin  
contribution was calculated using the ‘coupled-perturbed’ scheme as implemented in ORCA  
(see also refs 41–43). A single molecule was cut out of the chain of each compound presented in  
Table 6 by inserting hydrogen atoms at appropriate positions. These entities bear charge +1 for  
all species except **8**, which is neutral. The non-coordinated anions were not used, but for **1**  
calculations were performed both for a  $\mathbf{1}^+$  cation and a  $\mathbf{1}^-$  anion in which two  $\text{Cl}^-$  ions closest to  
Mn were taken into account. The differences in the calculated zero-field splitting parameters



were minuscule (Table 5). It is interesting to compare species **4** to **8**, because **8** has a coordinated SCN<sup>-</sup> ion, while in **4** SCN<sup>-</sup> is not coordinated, like anions in all other molecules. For **4**,  $D = -3.432 \text{ cm}^{-1}$ , and  $E = -0.528 \text{ cm}^{-1}$  were obtained. The  $D$  and  $E$  found in this way compare well to the experimental values in Table 4. The spin–spin contributions to  $D$  and  $E$  were  $-0.453 \text{ cm}^{-1}$  and  $-0.046 \text{ cm}^{-1}$ , respectively, while the spin–orbit coupling related contribution were  $-2.978 \text{ cm}^{-1}$  and  $-0.482 \text{ cm}^{-1}$ , respectively. The direction of the largest component ( $D_{zz}$ ) of the calculated  $D$  tensor was found 3.0 deg away from the long Mn–O<sub>alcohol</sub> bond, or 1.9 deg away from the normal to the least–squares NNOO plane of the Schiff base donor atoms. For **8**, the calculations produced  $D = -3.507 \text{ cm}^{-1}$ ,  $E = -0.578 \text{ cm}^{-1}$ . The spin–orbit contributions to  $D$  and  $E$  were  $-3.064 \text{ cm}^{-1}$  and  $-0.536 \text{ cm}^{-1}$ , respectively, while the spin–spin contributions were  $-0.443 \text{ cm}^{-1}$  and  $-0.042 \text{ cm}^{-1}$ . The replacement of an alcoholato ligand by SCN<sup>-</sup> thus does not cause the magnitude of  $D$  to change much. The calculated  $D_{zz}$  direction in **8** was found 1.7 deg away from the Mn–N<sub>thiocyanate</sub> bond, or 3.2 deg from the Mn–O<sub>alcohol</sub> bond (Fig. 9). The calculations, while reproducing well the experimental  $D$  magnitudes, fail to reproduce the substantially increased experimental  $E$  for **8** compared to **4**. Similar calculations, the results of which are presented in Table 5, show a narrow range of slightly overestimated  $D$  and slightly underestimated  $E$  values.

### The Mn–Mn interactions

The EPR spectra obtained in this work were in general of good quality, but were not as good as those previously obtained in this lab for some other Mn(III) systems.<sup>30,48,49</sup> The reason for this may be the interactions between the Mn(III) ions. The bridges between the manganese ions are not likely to transmit significant exchange interactions. A fragment containing two Mn ions was cut out of the chain of **4** and a broken–symmetry calculation<sup>50–53</sup> was performed. Similarly as in the calculations of  $D$  above, the ORCA software was employed using functional B3LYP with TZVPP functions for Mn and all coordinated atoms and SVP functions for all remaining atoms. The structures used for the broken–symmetry calculations are shown in the supplementary material. An exchange integral value  $J$  of just  $0.02 \text{ cm}^{-1}$  (antiferromagnetic, using the Heisenberg–Dirac–Van Vleck Hamiltonian in a form  $\mathbf{H} = J\mathbf{S}_1\mathbf{S}_2$ ) was obtained. The same value is obtained when calculating exchange interactions through the hydrogen bridges involving the SCN<sup>-</sup> ion in **4**. For **8**,  $J = 0.04 \text{ cm}^{-1}$  was calculated although the Mn–Mn distance in the chain of 6.695 Å was larger than in **4** (5.725 Å). It should be mentioned here that the magnitude of the exchange interactions depends less on the interatomic distance than on the nature of a bridge between the metal atoms. For example, a two orders of magnitude larger  $J$  of  $2.9 \text{ cm}^{-1}$  (translated to the notation used in this paper) was found in a Mn(III) dimer with slightly shorter Mn–Mn

distance than in our complexes, in which exchange is transmitted by a system of  $\pi$  bonds.<sup>54</sup> We performed a broken symmetry calculation using the published structure to obtain  $J$  of  $2.5 \text{ cm}^{-1}$ , in good agreement with experiment. It is noteworthy here, that the EPR spectra of **8** (Fig. S4) exhibit the most visible evidence of the metal–metal interactions in this series, in form of additional splittings observed on some resonances. Exchange interactions of this order of magnitude are indeed sufficient to split the EPR resonances in some Mn(III) dimers,<sup>55</sup> while they are not detectable in magnetic susceptibility measurements. The Mn–Mn distances in chains which are of the order of  $5.7 \text{ \AA}$  give rise to the dipole–dipole interactions of some  $-0.03 \text{ cm}^{-1}$ , comparable to the exchange interactions estimated above. Both dipolar and exchange effects are likely to affect the EPR linewidth, and may create additional spectral features. The metal–metal interactions in **8** occur in extended systems, unlike the discrete dimers studied in ref 55 and the problem seems impossible to be solved without using single–crystal EPR spectra.

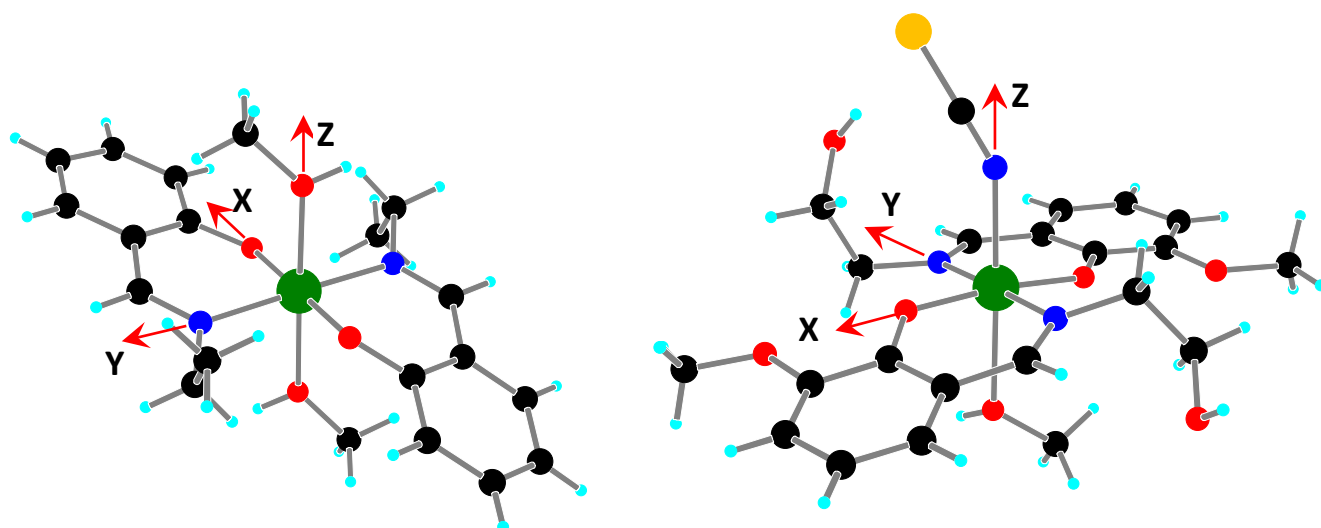


**Figure 9.** The structures of **4** (left) and **8** (right) used for the ORCA calculations and the D tensor axes directions resulting from calculations.

**Table 5. Experimental and calculated zero–field splitting parameters.**

Complex	$D_{\text{exp}}$ , $\text{cm}^{-1}$	$E_{\text{exp}}/D_{\text{exp}}$	$D_{\text{calc}}$ , $\text{cm}^{-1}$	$E_{\text{calc}}/D_{\text{calc}}$	$D_{\text{SO}}^1$ , $\text{cm}^{-1}$	$E_{\text{SO}}^1$ , $\text{cm}^{-1}$	$D_{\text{SS}}^2$ , $\text{cm}^{-1}$	$E_{\text{SS}}^2$ , $\text{cm}^{-1}$
<b>1</b>	-3.231	0.18	-3.464	0.13	-3.006	-0.457	-0.458	-0.036
<b>1</b> +2Cl <sup>-</sup>			-3.517	0.14	-3.065	-0.444	-0.452	-0.040
<b>2</b>	-3.223	0.17	-3.419	0.13	-2.958	-0.393	-0.461	-0.038
<b>3</b>	-3.197	0.16	-3.453	0.13	-2.991	-0.401	-0.462	-0.039
<b>4</b>	-3.296	0.20	-3.431	0.15	-2.978	-0.482	-0.453	-0.046
<b>5</b>	-3.271	0.20	-3.458	0.16	-3.005	-0.493	-0.453	-0.046

<b>8</b>	-3.44	0.21	-3.507	0.18	-3.064	-0.576	-0.443	-0.042
----------	-------	------	--------	------	--------	--------	--------	--------

<sup>1</sup>Spin-orbit coupling contribution. <sup>2</sup>Spin-spin contribution.

## Experimental section

### General Procedures

Reactions were carried out under air and using HPLC solvents. The IR spectra were done on ATR Bruker Vertex 70 spectrophotometer in the 4000–400 cm<sup>-1</sup> range. Elemental analyses were recorded using Flash 2000 Fisher Scientific Thermo Electron analyzer.

**EPR.** The high-field EPR spectra at temperatures ranging from ca. 3 K to 290 K were recorded on a home-built spectrometer at the EMR facility of the NHMFL.<sup>56</sup> The instrument is equipped with a superconducting magnet (Oxford Instruments) capable of reaching a field of 17 T. Microwave frequencies over the range 52–630 GHz were generated by a phase-locked Virginia Diodes source, producing a base frequency of 13±1 GHz, which was multiplied by a cascade of frequency multipliers. The instrument is a transmission-type device and uses no resonance cavity.

### Syntheses.

**{{Mn(HL<sup>1</sup>)<sub>2</sub>Cl}<sub>n</sub> (1)}** 2-Aminoethanol (0.36 ml, 6 mmol) and salicylaldehyde (0.56 g, 6 mmol) were added to 30 ml of methanol and stirred magnetically for 15 min until the colour of the solution turned in yellow. After manganese powder (0.11 g, 2 mmol) and NH<sub>4</sub>Cl (0.21 g, 4 mmol) were added to the solution, the reaction mixture was stirred at 50°C for ca 2 h. Total dissolution of manganese powder was observed. The dark brown crystals were collected after 1 day by filtration, washed with isopropanol and dried in air; yield 330 mg (39%, per Mn). The elemental analysis for C<sub>18</sub>H<sub>20</sub>N<sub>2</sub>O<sub>4</sub>ClMn (Mr = 418.76). Calcd: C, 51.63; H, 4.81; N, 6.69; Mn, 13.12%. Found: C, 51.55; H, 4.74; N, 6.55; Mn, 13.00%. IR (ATR, cm<sup>-1</sup>): 3155 (br), 2924 (w), 1612 (s), 1550 (s), 1441 (s), 1304 (s), 1218 (s), 1025 (m), 885 (m), 769 (s), 634 (m), 457 (s).

A different method of synthesis using manganese chloride tetrahydrate was reported previously.<sup>19</sup>

**{{Mn(HL<sup>1</sup>)<sub>2</sub>Br}<sub>n</sub> (2)}**. This complex was prepared in a way similar to that of **1**, but using NH<sub>4</sub>Br (0.39 g, 4 mmol) instead of NH<sub>4</sub>Cl. The dark brown crystals were collected after 1 day by filtration, washed with isopropanol and dried in air; yield 320 mg (35%, per Mn). The elemental analysis for C<sub>18</sub>H<sub>20</sub>N<sub>2</sub>O<sub>4</sub>BrMn (Mr = 463.20). Calcd: C, 46.67; H, 4.35; N, 6.05; Mn, 11.86%. Found: C, 46.54; H, 4.14; N, 5.85; Mn, 11.50%. IR (ATR, cm<sup>-1</sup>): 3151 (br), 2929 (w), 1607 (vs), 1546 (s), 1445 (s), 1300 (s), 1215 (s), 1025 (m), 884 (m), 767 (s), 638 (m), 456 (s).

**{{Mn(HL<sup>1</sup>)<sub>2</sub>I}<sub>n</sub> (3)}**. This complex was prepared in a way similar to that of **1**, but using NH<sub>4</sub>I (0.58 g, 4 mmol) instead of NH<sub>4</sub>Cl. The dark brown crystals were collected after 1 day by

1  
2 filtration, washed with isopropanol and dried in air; yield 410 mg (40%, per Mn). The elemental  
3 analysis for  $C_{18}H_{20}N_2O_4Mn$  (Mr = 510.20). Calcd: C, 42.37; H, 3.95; N, 5.49; Mn, 10.77%.  
4 Found: C, 42.15; H, 3.83; N, 5.24; Mn, 10.46%. IR (ATR,  $cm^{-1}$ ): 3149 (br), 2915 (w), 1607 (vs),  
5 1544 (s), 1439 (s), 1305 (s), 1218 (s), 1030 (m), 890 (m), 760 (m), 640 (m), 449 (s).  
6  
7

8  
9  **$\{[Mn(HL^1)_2]NCS\}_n$  (4)**. This complex was prepared in a way similar to that of **1**, but using  
10  $NH_4NCS$  (0.31 g, 4 mmol) instead of  $NH_4Cl$ . The dark brown crystals were collected after 1 day  
11 by filtration, washed with isopropanol and dried in air; yield 220 mg (25%, per Mn). The  
12 elemental analysis for  $C_{19}H_{20}N_3O_4SMn$  (Mr = 441.38). Calcd: C, 51.70; H, 4.57; N, 9.52; S,  
13 7.26; Mn, 12.44%. Found: C, 51.65; H, 4.28; N, 9.36; S, 7.15; Mn, 12.25%. IR (ATR,  $cm^{-1}$ ):  
14 3145 (br), 3056 (w), 2924 (w), 2071 (s), 1599 (vs), 1543 (s), 1444 (s), 1293 (m), 1219 (m), 1025  
15 (m), 885 (m), 757 (s), 683 (m), 456 (s).  
16  
17  
18  
19

20  
21  **$\{[Mn(HL^2)_2]Cl\}_n$  (5)**. This complex was prepared in a way similar to that of **1**, but using *o*-  
22 vanillin (0.94 g, 6 mmol) instead of salicylaldehyde. The dark brown precipitate was collected  
23 after 1 day by filtration, washed with isopropanol and dried in air; yield 212 mg (43%, per Mn).  
24 The elemental analysis for  $C_{20}H_{24}N_2O_6ClMn$  (Mr = 487.81). Calcd: C, 50.17; H, 5.05; N, 5.85;  
25 Mn, 11.47%. Found: C, 50.05; H, 4.97; N, 5.74; Mn, 11.35%. IR (ATR,  $cm^{-1}$ ): 3434(br), 3396  
26 (w), 3186 (br), 2936 (w), 1607 (vs), 1551 (m), 1469 (s), 1300 (m), 1249 (s), 1029 (m), 864 (s),  
27 744 (s), 640 (m), 453 (m).  
28  
29  
30  
31  
32

33 It should be noted that that **5** can be also obtained by the ordinary method of synthesis using  
34 manganese chloride tetrahydrate instead of manganese powder and ammonium chloride.  
35

36  
37  **$\{[Mn(HL^2)_2]Br\}_n$  (6)**. This complex was prepared in a way similar to that of **5**, but using  $NH_4Br$   
38 (0.39 g, 4 mmol) instead of  $NH_4Cl$ . The dark brown precipitate was collected after 1 day by  
39 filtration, washed with isopropanol and dried in air; yield 320 mg (31%, per Mn). The elemental  
40 analysis for  $C_{20}H_{24}N_2O_6BrMn$  (Mr = 523.26). Calcd: C, 45.91; H, 4.62; N, 5.35; Mn, 10.50%.  
41 Found: C, 45.75; H, 4.52; N, 5.27; Mn, 10.35%. IR (ATR,  $cm^{-1}$ ): 3437 (br), 3393 (w), 3184 (br),  
42 2931 (w), 1610 (vs), 1548 (m), 1473 (s), 1315 (m), 1239 (s), 1019 (m), 867 (s), 746 (s), 645 (m),  
43 455 (m).  
44  
45  
46  
47

48  **$\{[Mn(HL^2)_2]I\}_n$  (7)**. The synthesis of the complex **7**, was previously reported by our group.<sup>17</sup>

49  
50  **$[Mn(HL^2)_2(NCS)]$  (8)**. This complex was prepared in a way similar to that of **1**, but using *o*-  
51 vanillin (0.94 g, 6 mmol) instead of salicylaldehyde and  $NH_4NCS$  (0.31 g, 4 mmol) instead of  
52  $NH_4Cl$ . Yellow crystals were collected after 1 days by filtration, washed with isopropanol and  
53 dried in air; yield 300 mg (30%, per Mn). The elemental analysis for  $C_{21}H_{24}N_3O_6SMn$  (Mr =  
54 501.43). Calcd: C, 50.30; H, 4.82; N, 8.38; S, 6.39; Mn, 10.96%. Found: C, 50.16; H, 4.64; N,  
55 7.98; S, 6.12; Mn, 11.30%. FT-IR (KBr,  $v_{max}$   $cm^{-1}$ ): 3420 (br), 2919 (w), 2071 (vs), 1616 (vs),  
56 1553 (m), 1475 (s), 1452(s), 1399 (m), 1353(w), 1303 (vs), 1227(s), 1193(m), 1112 (w),  
57  
58  
59  
60

1086(m), 1055(m), 1024(m), 979 (m), 902 (w), 864 (s), 784 (w), 742(s), 639(s), 590(w), 528(w), 471(w).

### X-ray structure determination

Single crystal X-ray diffraction data were collected on an Agilent Technologies SuperNova diffractometer equipped with AtlasCCD detector and micro-focus Cu-K $\alpha$  radiation ( $\lambda=1.54184$  Å). The structures were solved by direct methods and refined on  $F^2$  by full matrix least-squares techniques using SHELX97 (G.M. Sheldrick, 1998) package. All non-H atoms were refined anisotropically and multiscan empirical absorption was applied using CrysAlisPro program (CrysAlisPro, AgilentTechnologies, V1.171.38.41r, 2015). The hydrogen atoms were included in the geometrically calculated position and refined riding on the corresponding atom. A summary of the crystallographic data and the structure refinement is given in Table 6. CCDC 1842146 (**1**), 1842148 (**2**), 1842149 (**3**), 1842147 (**4**), 1854314 (**8**) contain the supplementary crystallographic data for this paper. This data can be obtained free of charge from The Cambridge Crystallographic Data Centre via [www.ccdc.cam.ac.uk/data\\_request/cif](http://www.ccdc.cam.ac.uk/data_request/cif).

**Table 6.** Crystallographic data, details of data collection and structure refinement parameters

	<b>2</b>	<b>3</b>	<b>4</b>	<b>8</b>
Formula	C <sub>18</sub> H <sub>20</sub> N <sub>2</sub> O <sub>4</sub> BrMn	C <sub>18</sub> H <sub>20</sub> N <sub>2</sub> O <sub>4</sub> IMn	C <sub>19</sub> H <sub>20</sub> N <sub>3</sub> O <sub>4</sub> SMn	C <sub>21</sub> H <sub>24</sub> N <sub>3</sub> O <sub>6</sub> SMn
M [g·mol <sup>-1</sup> ]	463.20	510.20	441.38	501.43
T [K]	150.00(10)	150.01(10)	150.00(10)	295.65(10)
Crystal system	monoclinic	monoclinic	orthorhombic	monoclinic
Space group	C 2/c	C 2/c	P 2 <sub>1</sub> 2 <sub>1</sub> 2 <sub>1</sub>	P 2 <sub>1</sub> /n
a [Å]	18.5786(9)	19.3631(5)	5.7247(3)	10.8561(6)
b [Å]	5.7196(3)	5.7552(2)	16.7646(7)	11.6732(5)
c [Å]	18.1494(10)	17.9767(5)	20.4425(8)	17.5981(9)
$\alpha$ [°]	90	90	90	90
$\beta$ [°]	105.278(5)	102.470(3)	90	96.457(5)
$\gamma$ [°]	90	90	90	90
V [Å <sup>3</sup> ]	1860.44(17)	1956.04(10)	1961.91(15)	2215.98(19)
Z	4	4	4	4
$\rho_{\text{calcd}}$ [g·cm <sup>-3</sup> ]	1.654	1.732	1.494	1.503
$\mu$ [mm <sup>-1</sup> ]	8.513	18.096	6.733	6.104
Goodness-of-fit on $F^2$	1.043	1.036	1.087	1.035
$F(000)$	936	1008	912	1040
$\theta_{\text{min}}/\theta_{\text{max}}$ , (deg)	4.935/72.279	4.678/72.593	3.409/72.241	4.4640/73.1450
Final $R_1/wR_2$ [ $I > 2\sigma(I)$ ]	0.0256/0.0641	0.0192/0.0469	0.0373/0.0918	0.0333/0.0824
$R_1/wR_2$ (all data)	0.0303/ 0.0672	0.0207/0.0477	0.0408/0.1003	0.0401/0.0871

largest diff. peak and hole (e Å <sup>-3</sup> )	0.346/−0.244	0.379/−0.422	0.304/−0.394	0.259/−0.330
--	--------------	--------------	--------------	--------------

## Conclusions

A series of chain polymeric complexes with the general formula  $\text{Mn}^{\text{III}}(\text{HL})_2\text{X}$ , where  $\text{H}_2\text{L}$  ligands are Schiff bases derived from salicylaldehyde or *o*-vanillin and 2-aminoethanol and X are Cl, Br, I and NCS, were prepared *via* simple and productive “direct synthesis” approach based on one-pot reaction between manganese powder, ammonium salt and organic ligand formed in situ in methanol solution. X-ray analysis revealed two types of chain polymeric crystal structure for the obtained complexes: (1) the cationic chain structure consisting of the polymer cations  $[\text{Mn}(\text{HL}^{1,2})_2]_n^+$  and counter ions  $\text{X}^-$ , in compounds **1–7**, and (2) the molecular chain structure built of neutral polymeric molecules  $[\text{Mn}(\text{HL}^2)_2(\text{NCS})]_n$ , in **8**. The metal centers inside the cationic chain are bridged through two  $\{-\text{NCCO}-\}$  fragments with linear  $\{\text{Mn}\}_n$  arrangement while in the molecular chain they are linked with one NCCO-bridge forming the zig-zag metal atom arrangement. High-field EPR spectroscopy was used to determine accurately the zero-field splitting parameters and was supported by DFT calculations. The data obtained are correlated with crystallographic results and demonstrate that the generally more distorted structures in compounds of ligand L2 compared to L1 give rise to larger *E* parameters in the former. The DFT calculations suggest presence of very weak antiferromagnetic exchange interactions between Mn ions, which are stronger in complex **8** ( $0.04 \text{ cm}^{-1}$ ), containing coordinated SCN<sup>-</sup> anions, than in other compounds (like  $J=0.02 \text{ cm}^{-1}$  in **4**). They are presumably transmitted by the hydrogen bonds and seem to affect the HF EPR spectra of **8**, but they cannot make our compounds single chain magnets because of their expected antiferromagnetic character.

## Supporting Material Available:

The Supporting Information is available free of charge on the ACS Publications website at DOI:xxx, which include: HFEPR spectra of **1–3**, and **5–8**, the arrangements of the Mn moieties used to calculate the exchange integrals in **4** and **8**.

## Notes

The authors declare no competing financial interest.

## Acknowledgements

This work was supported in France by the CNRS, the University of Angers, the French Embassy in Kiev (grants to O.S. and N.P.) and the Ministry of Education and Science of Ukraine (Project no. 19BF037–05). The high–field EPR spectra were recorded at the NHMFL, which is funded by the NSF through the Cooperative Agreement No. DMR–1644779 and the State of Florida. E.G. gratefully acknowledges the Slovenian Research Agency (ARRS) for the financial support of the present study within the research program P1–0045 Inorganic Chemistry and Technology.

## Author Contributions

The manuscript was written through contributions of all authors. All authors have given approval to the final version of the manuscript.

## ORCID

Oleh Stetsiuk: 0000–0003–3269–7466

Narcis Avarvari: 0000–0001–9970–4494

Evgeny Goreschnik: 0000–0002–4675–2190

Vladimir Kokozay: 0000–0003–1834–3020

Svitlana Petrusenko: 0000–0001–8594–2643

Andrew Ozarowski: 0000–0001–6225–9796

## References

- (1) Rutherford, A. W.; Boussac, A., Water Photolysis in Biology. *Science* **2004**, *303*, 1782–1784.
- (2) Gupta, R.; Taguchi, T.; Lassalle–Kaiser B.; Bominaar, E. L.; Yano, J.; Hendrich, M. P.; Borovik, A. S. High–Spin Mn–Oxo Complexes And Their Relevance to the Oxygen–Evolving Complex Within Photosystem II. *PNAS* **2015**, *112*, 5319–5324.
- (3) Tao, L.; Stitch, T. A.; Soldatova, A. V.; Tebo, B. M.; Spiro, T. G.; Casey, W. H.; Britt, R. D. Mn(III) Species Formed by the Multi–Copper Oxidase MnxG Investigated by Electron Paramagnetic Resonance Spectroscopy. *J. Biol. Inorg. Chem.* **2018**, *23*, 1093–1104.
- (4) Sessoli, R.; Gatteschi, D.; Caneschi, A.; Novak, M.A., Magnetic bistability in a metal–ion cluster, *Nature* **1993**, *365*, 141–143.
- (5) Boskovic, C.; Bircher, R.; Tregenna–Piggott, P. L. W.; Güdel, H. U.; Paulsen, C.; Wernsdorfer, W.; Barra, A. L.; Khatsko, E.; Neels, A.; Sfoeckli–Evans, H. Ferromagnetic and Antiferromagnetic Intermolecular Interactions in a New Family of Mn<sub>4</sub> Complexes with an Energy Barrier to Magnetization Reversal. *J. Am. Chem. Soc.* **2003**, *125*, 14046–14058.

- 1  
2  
3  
4  
5  
6  
7  
8  
9  
10  
11  
12  
13  
14  
15  
16  
17  
18  
19  
20  
21  
22  
23  
24  
25  
26  
27  
28  
29  
30  
31  
32  
33  
34  
35  
36  
37  
38  
39  
40  
41  
42  
43  
44  
45  
46  
47  
48  
49  
50  
51  
52  
53  
54  
55  
56  
57  
58  
59  
60
- (6) Realista, S.; Fitzpatrick, A. J.; Santos, G.; Ferreira, L. P.; Barroso, S.; Pereira, L. C. J.; Bandeira, N. A. G.; Neugebauer, P.; Hruby, J.; Morgan, G. G.; van Slageren, J.; Calhorda, M. J.; Martinho, P. N. A Mn(III) single ion magnet with tridentate Schiff–base ligands. *Dalton Trans.* **2016**, *45*, 12301–12307.
- (7) Dolai, M.; Mondal, A.; Liu, J.–L.; Ali, M. Three Novel Mononuclear Mn(III)–Based Magnetic Materials With Square Pyramidal Versus Octahedral Geometries. *New J. Chem.* **2017**, *41*, 10890–10898.
- (8) Ishikawa, R.; Miyamoto, R.; Nojiri, H.; Breedlowe, B. K.; Yamashita, M. Slow Relaxation of the Magnetization of an Mn<sup>III</sup> Single Ion. *Inorg. Chem.* **2013**, *52*, 8300–8302
- (9) Vallejo, J.; Pascual–Alvarez, A.; Cano, J.; Castro, I.; Julve, M.; Lloret, F.; Krzystek, J.; De Munno, G.; Armentano, D.; Wernsdorfer, W.; Ruiz–Garcia, R.; Pardo, E. Field–Induced Hysteresis and Quantum Tunneling of the Magnetization in a Mononuclear Manganese(III) Complex. *Angew. Chem. Int. Ed.* **2013**, *52*, 14075–14079.
- (10) Sun, H. L.; Wang, Z.M.; Gao, S., Strategies towards single–chain magnets, *Coord. Chem. Rev.* **2010**, *254*, 1081–1100.
- (11) Bar, A. K.; Pichon, C.; Sutter, J. P. Magnetic anisotropy in two– to eight–coordinated transition–metal complexes: recent developments in molecular magnetism, *Coord. Chem. Rev.* **2016**, *308*, 346–380.
- (12) Giannopoulos, D. P.; Thuijs, A.; Wernsdorfer, W.; Pilkington, M.; Christou, G.; Stamatatos, T.C., Supramoleculr chains of high nuclearity {Mn<sup>III</sup><sub>25</sub>} barrel–like single molecule magnets, *Chem. Commun.* **2014**, *50*, 779–781.
- (13) Silha, T.; Nemeč, I.; Herchel, R.; Travnichek, Z., Structural and magnetic characterizations of the first manganese(III) Schiff base complexes involving hexathiocyanidoplatinate(IV) bridges *Cryst. Eng. Comm.* **2013**, *15*, 5351–5358.
- (14) Weatherburn, D.C.; Mandal, S.; Mukhopadhyay, S.; Bhaduri, S.; Lindoy, L.F., *Manganese, in Comprehensive Coordination Chemistry II: From Biology to Nanotechnology*. Second Edition, Volume 5, ed. E.C. Constable, J.R.Dilworth, Elsevier, **2005**.
- (15) Stetsiuk, O.; Synytsia, V.; Petrusenko, S. R.; Kokozay, V. N.; El–Ghayoury, A.; Cano, J.; Lloret, F.; Julve, M.; Fleury, B.; Avarvari, N., Co–existence of ferro– and antiferromagnetic interactions in a hexanuclear mixed–valence Co<sup>III</sup><sub>2</sub>Mn<sup>II</sup><sub>2</sub>Mn<sup>IV</sup><sub>2</sub> cluster sustained by a multidentate Schiff base ligand, *Dalton Trans.* **2019**, *48*, 11862–11871.
- (16) Nesterova, O. V.; Chygorin, E. N.; Omelchenko, I. V.; Shishkin, O. V.; Boča, R.; Pombeiro A. J. L., A self–assembled octanuclear complex bearing the uncommon close–packed {Fe<sub>4</sub>Mn<sub>4</sub>(μ<sub>4</sub>–O)<sub>4</sub>(μ–O)<sub>4</sub>} molecular core, *Dalton Trans.* **2015**, *44*, 14918–14924.
- (17) Kokozay, V. N.; Vassilyeva, O. Y.; Makhankova, V. G. (2018). *Direct Synthesis of Metal Complexes*, edited by B. Kharisov, pp. 183–237. Amsterdam: Elsevier.
- (18) Nesterov, D. S.; Nesterova, O. V.; Kokozay, V. N.; Pombeiro A. J. L., Polynuclear Heterometallic Complexes from Metal Powders: The “Direct Synthesis” Approach. *Eur. J. Inorg. Chem.* **2014**, *27*, 4496–4517.
- (19) Zhang, L.F.; Ni, Z.H.; Zong, Z.M.; Wei, X.Y.; Ge, C.H.; Kou, H.Z., A novel one–dimensional complex: catena–poly–[[manganese(III)–di–μ–2–[(2–hydroxy–ethyl)–imino–methyl]–phenolato–κ<sup>2</sup>O<sup>1</sup>,N:κO<sup>2</sup>;κO<sup>2</sup>:κ<sup>2</sup>O<sup>1</sup>]chloride], *Acta Cryst.* **2005**, *C61*, m542–m544.
- (20) Petrusenko, S. R.; Stetsyuk, O. M.; Omelchenko, I. V., Catena–Poly[[manganese(III)–bis–{[μ]–2–[(2–hydroxy–eth–yl)imino–meth–yl]–6–meth–oxy–phenolato–κ<sup>3</sup>O<sup>1</sup>,N:O<sup>2</sup>;κ<sup>3</sup>O<sup>2</sup>:N,O<sup>1</sup>}] iodide], *Acta Cryst.* **2013**, *E69*, m326–m327.



- 1  
2 (21) Brown, I. D.; Altermatt, D. Bond–Valence Parameters Obtained from a Systematic  
3 Analysis of the Inorganic Crystal Structure Database. *Acta Cryst B* **1985**, *41*, 244–247.  
4  
5 (22) Thorp, H. H. Bond Valence Sum Analysis of Metal–Ligand Bond Lengths in  
6 Metalloenzymes and Model Complexes. *Inorg. Chem.* **1992**, *31*, 1585–1588.  
7  
8 (23) Coxall, R. A.; Harris, S. G.; Henderson, D. K.; Parsons, S.; Tasker, P. A.; Winpenny, R. E.  
9 P., Inter–ligand reactions: in situ formation of new polydentate ligands, *J. Chem. Soc.,*  
10 *Dalton Trans.*, **2000**, 2349–2356.  
11  
12 (24) Collin, R. J.; Smith, B. C. Ionic Radii for Group 1 Halide Crystals and Ion–Pairs. *Dalton*  
13 *Trans.* **2005**, *4*, 702–705.  
14  
15 (25) Campbell, K. A.; Force, D. A.; Nixon, P. J.; Dole, F.; Diner, B. A.; Britt, R. D. Dual–Mode  
16 EPR Detects the Initial Intermediate in Photoassembly of the Photosystem II Mn Cluster:  
17 The Influence of Amino Acid Residue 170 of the D1 Polypeptide on Mn Coordination. *J.*  
18 *Am. Chem. Soc.* **2000**, *122*, 3754–3761.  
19  
20 (26) Campbell, K. A.; Lashley, M. R.; Wyatt, J. K.; Nantz, M. H.; Britt, R. D. Dual–Mode EPR  
21 Study of Mn(III) Salen and the Mn(III) Salen–Catalyzed Epoxidation of *cis*- $\alpha$ -  
22 Methylstyrene. *J. Am. Chem. Soc.* **2001**, *123*, 5710–5719.  
23  
24 (27) Gupta, R.; Taguchi, T.; Borovik, A. S.; Hendrich, M. P. Characterization of Monomeric  
25 MnII/III/IV–Hydroxo Complexes from X– and Q–Band Dual Mode Electron Paramagnetic  
26 Resonance (EPR) Spectroscopy. *Inorg. Chem.* **2013**, *52*, 12568–12575.  
27  
28 (28) Westphal, A.; Klinkebiel, A.; Berends, H. M.; Broda, H.; Kurz, P.; Tuzcek, F. Electronic  
29 Structure and Spectroscopic Properties of Mononuclear Manganese(III) Schiff Base  
30 Complexes: A Systematic Study on [Mn(acen)X] Complexes by EPR, UV/vis, and MCD  
31 Spectroscopy (X =Hal, NCS). *Inorg. Chem.* **2013**, *52*, 2372–2387.  
32  
33 (29) Oswald, V. F.; Weitz, A. C.; Biswas, S.; Ziller, J. W.; Hendrich, M. P.; Borovik, A. S.  
34 Manganese – Hydroxido Complexes Supported by a Urea/Phosphinic Amide Tripodal  
35 Ligand. *Inorg. Chem.* **2018**, *57*, 13341–13350.  
36  
37 (30) Aromi, G.; Telser, J.; Ozarowski, A.; Brunel, L. C.; Stoeckli–Evans, H. M.; Krzystek, J.  
38 Synthesis, Crystal Structure, and High–Precision High–Frequency and –Field Electron  
39 Paramagnetic Resonance Investigation of a Manganese(III) Complex:  
40 [Mn(dbm)<sub>2</sub>(py)<sub>2</sub>](ClO<sub>4</sub>). *Inorg. Chem.* **2005**, *44*, 187–196.  
41  
42 (31) Duboc, C. Determination and Prediction of The Magnetic Anisotropy of Mn Ions. *Chem.*  
43 *Soc. Rev.* **2016**, *45*, 5834–5847.  
44  
45 (32) Arauzo, A.; Bartolomé, E.; Benniston, A. C.; Melnic, S.; Shova, S.; Luzón, J.; Alonso, P.  
46 J.; Barra, A. L.; Bartolomé, J. Slow Magnetic Relaxation In A Dimeric Mn<sub>2</sub>Ca<sub>2</sub> Complex  
47 Enabled By The Large Mn(III) Rhombicity. *Dalton Trans.*, **2017**, *46*, 720–732.  
48  
49 (33) Konstantatos, A.; Bewley, R.; Barra, A. L.; Bendix, J.; Piligkos, S.; Weihe, H. In–Depth  
50 Magnetic Characterization of a [2 × 2] Mn(III) Square Grid Using SQUID Magnetometry,  
51 Inelastic Neutron Scattering, and High Field Electron Paramagnetic Resonance  
52 Spectroscopy. *Inorg. Chem.* **2016**, *55*, 10377–10382.  
53  
54 (34) Ozarowski, A. The Zero–Field–Splitting Parameter D in Binuclear Copper(II) Carboxylates  
55 Is Negative. *Inorg. Chem.*, **2008**, *47*, 9760–9762.  
56  
57 (35) Ozarowski, A.; Calzado, C. J.; Sharma, R. P.; Kumar, S.; Jezierska, J.; Angeli, C.; Spizzo,  
58 F.; Ferretti, V. Metal–Metal Interactions in Trinuclear Copper(II) Complexes  
59 [Cu<sub>3</sub>(RCOO)<sub>4</sub>(H<sub>2</sub>TEA)<sub>2</sub>] and Binuclear [Cu<sub>2</sub>(RCOO)<sub>2</sub>(H<sub>2</sub>TEA)<sub>2</sub>]. Syntheses and Combined  
60

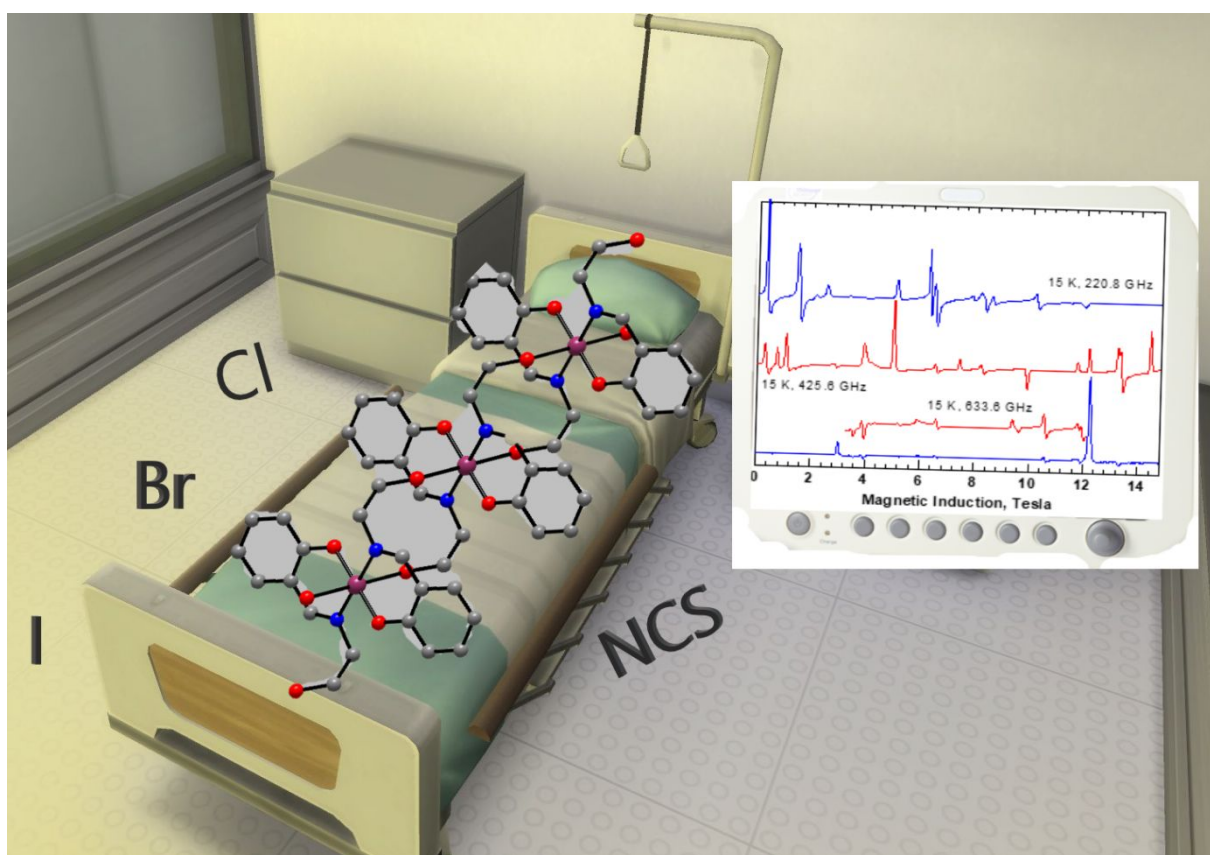
- 1  
2 Structural, Magnetic, High-Field Electron Paramagnetic Resonance, and Theoretical  
3 Studies. *Inorg. Chem.*, **2015**, *54*, 11916–11934.
- 4  
5 (36) Ozarowski, A.; Szymanska, I.B.; Muziol, T.; Jezierska, J. High-Field EPR and Magnetic  
6 Susceptibility Studies on Binuclear and Tetranuclear Copper Trifluoroacetate Complexes.  
7 X-ray Structure Determination of Three Tetranuclear Quinoline Adducts of Copper(II)  
8 Trifluoroacetate. *J. Am. Chem. Soc.*, **2009**, *131*, 10279–10292.
- 9  
10 (37) Boca, R. Zero-field splitting in metal complexes. *Coord. Chem. Rev.* **2004**, *248*, 757–815.
- 11  
12 (38) Boca, R. Magnetic Parameters and Magnetic Functions in Mononuclear Complexes Beyond  
13 the Spin-Hamiltonian Formalism. *Struct. Bond.* **2006**, *117*, 1–264.
- 14  
15 (39) Tadyszak, K.; Rudowicz, C.; Ohta, H.; Sakurai, T. Electron magnetic resonance data on  
16 high-spin Mn(III; S= 2) ions in porphyrinic and salen complexes modeled by microscopic  
17 spin Hamiltonian approach. *J. Inorg. Biochem.* **2017**, *175*, 36–46.
- 18  
19 (40) Mossin, S.; Weihe, H.; Barra, A. L. Is the Axial Zero-Field Splitting Parameter of  
20 Tetragonally Elongated High-Spin Manganese(III) Complexes Always Negative?. *J. Am.*  
21 *Chem. Soc.* **2002**, *124*, 8764–8765.
- 22  
23 (41) Shova, S.; Vlad, A.; Cazacu, M.; Krzystek, J.; Bucinski, L.; Breza, M.; Darvasiova, D.;  
24 Rapta, P.; Cano, J.; Telser, J.; Arion, V. B. A five-Coordinate Manganese(III) Complex Of  
25 A Salen Type Ligand With A Positive Axial Anisotropy Parameter D. *Dalton Trans.*, **2017**,  
26 *46*, 11817–11829.
- 27  
28 (42) Duboc, C.; Ganyushin, D.; Sivalingam, K.; Collomb, M.-N.; Neese, F. Systematic  
29 Theoretical Study of the Zero-Field Splitting in Coordination Complexes of Mn(III).  
30 Density Functional Theory versus Multireference Wave Function Approaches. *J. Phys.*  
31 *Chem. A* **2010**, *114*, 10750–10758.
- 32  
33 (43) Pascual-Alvarez, A.; Vallejo, J.; Pardo, E.; Julve, M.; Lloret, F.; Krzystek, J.; Armentano,  
34 D.; Wernsdorfer, W.; Cano, J. Field-Induced Slow Magnetic Relaxation in a Mononuclear  
35 Manganese(III)-Porphyrin Complex. *Chem. Eur. J.* **2015**, *21*, 17299–1730.
- 36  
37 (44) Schäfer, A.; Horn, H.; Ahlrichs, R. Fully Optimized Contracted Gaussian Basis Sets for  
38 Atoms Li to Kr. *J. Chem. Phys.* **1992**, *97*, 2571–2577.
- 39  
40 (45) The Ahlrichs auxiliary basis sets were obtained from the TurboMole basis set library under  
41 <ftp://chemie.uni-karlsruhe.de/pub/jbasen>.
- 42  
43 (46) Eichkorn, K.; Weigend, F.; Treutler, O.; Ahlrichs, R. Auxiliary Basis Sets for Main Row  
44 Atoms and Transition Metals and Their Use to Approximate Coulomb Potentials. *Theor.*  
45 *Chem. Accounts Theory, Comput. Model. (Theoretica Chim. Acta)* **1997**, *97*, 119–124.
- 46  
47 (47) Neese, F. *ORCA – An Ab Initio, Density Functional and Semiempirical Program Package*,  
48 Version 4.0.1; Surf Sara: Amsterdam **2017**. Neese, F. The ORCA Program System. *Wiley*  
49 *Interdiscip. Rev. Comput. Mol. Sci.* **2012**, *2*, 73–78.
- 50  
51 (48) Harvey, J. D.; Ziegler, C. J.; Telser, J.; Ozarowski, A. and Krzystek, J. High-Frequency  
52 and -Field EPR Investigation of a Manganese(III) N-Confused Porphyrin Complex,  
53 [Mn(NCTPP)(py)<sub>2</sub>]. *Inorg. Chem.* **2005**, *44*, 4451–4453.
- 54  
55 (49) Field-induced slow magnetic relaxation in a mononuclear manganese(III) porphyrin  
56 Pascual-Álvarez, A.; Vallejo, J.; Pardo, E.; Julve, M.; Lloret, F.; Krzystek, J.; Armentano,  
57 D.; Wernsdorfer, W. and Cano, J. *Chem. Eur. J.* **2015**, *21*, 17299–17307.
- 58  
59 (50) Noodleman, L. Valence Bond Description of Antiferromagnetic Coupling in Transition  
60 Metal Dimers. *J. Chem. Phys.* **1981**, *74*, 5737–5743.

- 1  
2 (51) Noodleman, L.; Davidson, E. R. Ligand Spin Polarization and Antiferromagnetic Coupling  
3 in Transition Metal Dimers. *Chem. Phys.* **1986**, *109*, 131–143.  
4  
5 (52) Malrieu, J. P.; Caballol, R.; Calzado, C. J.; de Graaf, C.; Guihéry, N. Magnetic Interactions  
6 in Molecules and Highly Correlated Materials: Physical Content, Analytical Derivation, and  
7 Rigorous Extraction of Magnetic Hamiltonians. *Chem. Rev.* **2014**, *114*, 429–492.  
8  
9 (53) Rodríguez-Fortea, A.; Alemany, P.; Alvarez, S.; Ruiz, E. Exchange Coupling in Halo-  
10 Bridged Dinuclear Cu(II) Compounds: A Density Functional Study. *Inorg. Chem.* **2002**, *41*,  
11 3769–3778.  
12  
13 (54) Aromi, G.; Gamez, P.; Roubeau, O.; Carrero Berzal, P.; Kooijman, H.; Spek, A. L.;  
14 Driessen, W. L.; Reedijk, J. A Solvent-Controlled Switch of Manganese Complex  
15 Assemblies with a  $\beta$ -Diketonate-Based Ligand. *Inorg. Chem.* **2002**, *41*, 3673–3683  
16  
17 (55) Shova, S.; Vlad, A.; Cazacu, M.; Krzystek, J.; Ozarowski, A.; Malček, M.; Bucinski, L.;  
18 Rapta, P.; Cano, J.; Telser, J.; Arion, V. B. Dinuclear manganese(III) complexes with  
19 bioinspired coordination and variable linkers showing weak exchange effects: a synthetic,  
20 structural, spectroscopic and computation study. *Dalton Trans.* **2019**, *48*, 5909–5922.  
21  
22 (56) Hassan, A. .; Pardi, L. .; Krzystek, J.; Sienkiewicz, A.; Goy, P.; Rohrer, M.; Brunel, L.-C.  
23 Ultrawide Band Multifrequency High-Field EMR Technique: A Methodology for  
24 Increasing Spectroscopic Information. *J. Magn. Reson.* **2000**, *142*, 300–312.  
25  
26  
27  
28  
29  
30  
31  
32  
33  
34  
35  
36  
37  
38  
39  
40  
41  
42  
43  
44  
45  
46  
47  
48  
49  
50  
51  
52  
53  
54  
55  
56  
57  
58  
59  
60

1  
2 For Table of Contents Use Only  
3  
4  
5

6  
7 **Mn(III) Chain Coordination Polymers assembled by Salicylidene–2–**  
8 **ethanolamine Schiff Base Ligands: Synthesis, Crystal Structures and HFEPR**  
9  
10 **Study**  
11  
12  
13  
14

15 Oleh Stetsiuk<sup>a</sup>, Nataliya Plyuta<sup>a,c</sup>, Narcis Avarvari<sup>a</sup>, Evgeny Goreshnik<sup>b</sup>, Vladimir Kozozay<sup>c</sup>,  
16 Svitlana Petrusenko<sup>\*c</sup>, and Andrew Ozarowski<sup>\*d</sup>  
17  
18  
19



49 Syntheses, crystal structures and high-field EPR measurements of Mn(III) polymeric complexes  
50 are discussed. Theoretical calculations suggest presence of weak antiferromagnetic exchange  
51 interactions between Mn ions.  
52  
53  
54  
55  
56  
57  
58  
59  
60